IOP Publishing and International Atomic Energy Agency Nuclear Fusion
Nucl. Fusion **53** (2013) 043017 (7pp) doi:10.1088/0029-5515/53/4/043017

Internal amplitude, structure and identification of compressional and global Alfvén eigenmodes in NSTX

N.A. Crocker[1], E.D. Fredrickson[2], N.N. Gorelenkov[2], W.A. Peebles[1], S. Kubota[1], R.E. Bell[2], A. Diallo[2], B.P. LeBlanc[2], J.E. Menard[2], M. Podestà[2], K. Tritz[3] and H. Yuh[4]

[1] Department of Physics and Astronomy, University of California, Los Angeles, CA 90095, USA
[2] Princeton Plasma Physics Laboratory, Princeton, NJ 08543, USA
[3] Department of Physics and Astronomy, The Johns Hopkins University, Baltimore, MD 21218, USA
[4] Nova Photonics, Princeton, NJ 08543, USA

E-mail: ncrocker@physics.ucla.edu

Received 17 December 2012, accepted for publication 13 March 2013
Published 28 March 2013
Online at stacks.iop.org/NF/53/043017

Abstract
Fast-ions (e.g. fusion alphas and neutral beam ions) will excite a wide range of instabilities in ITER and a Fusion Nuclear Science Facility device. Among the possible instabilities are high frequency Alfvén eigenmodes (AEs) excited through Doppler-shifted cyclotron resonance with beam ions. High frequency AEs cause fast-ion transport, correlate with enhanced electron thermal transport and are postulated to contribute to ion heating. These high frequency modes have historically been identified as a mixture of compressional (CAE) and global (GAE) Alfvén eigenmodes, but distinguishing between the CAEs and GAEs has sometimes proven difficult. Identification is essential for understanding the extent of their effect, since the two types of modes have very different effects on resonant particle orbits. The effect on plasma performance of high frequency AEs is investigated in NSTX, facilitated by a recently upgraded array of 16 fixed-frequency quadrature reflectometers. Detailed measurements of high frequency AE amplitude and eigenmode structure were obtained in a high power (6 MW), beam-heated H-mode plasma that is very similar to those in which high frequency AE activity is shown to correlate with enhanced electron thermal transport. These measurements, which extend from the plasma edge to deep in the core, can be used in modelling the effects of the modes on electron thermal transport. The observed modes are identified by comparison of their frequency and measured toroidal mode numbers with local Alfvén dispersion relations. The modes identified as CAEs have higher frequencies (predominantly $f >\sim 600$ kHz) and smaller toroidal mode numbers ($|n| \leqslant 5$) than the GAEs (predominantly $f <\sim 600$ kHz, $n = -6$ to -8). Also, they are strongly core localized, in contrast with the GAEs, which also peak towards the plasma centre but have much broader radial extent.

(Some figures may appear in colour only in the online journal)

1. Introduction

Fast-ions (e.g. fusion alphas and neutral beam ions) will excite a wide range of instabilities in ITER and a Fusion Nuclear Science Facility device. Among the possible instabilities are high frequency Alfvén eigenmodes (AEs) excited through Doppler-shifted cyclotron resonance with beam ions [1]. High frequency AEs cause fast-ion transport [2–4], correlate with enhanced electron thermal transport [5] and are postulated to contribute to ion heating [6]. Historically, various attempts have been made to identify these high frequency modes, leading to the conclusion that they are a mixture of compressional (CAE) and global (GAE) Alfvén eigenmodes [1–3, 7]. However, distinguishing CAEs from GAEs has sometimes proven difficult [3]. Identification is essential for understanding the extent of their effect, since the two types of modes have very different effects on resonant particle orbits. The effect on plasma performance of high frequency AEs is investigated in NSTX. A recently upgraded array of 16 fixed-frequency quadrature reflectometers has facilitated this investigation, yielding detailed measurements of high frequency AE amplitude and eigenmode structure (see figure 1) in a high power (6 MW), beam-heated H-mode plasma (shot 141398) [8]. The plasma investigated is very similar to

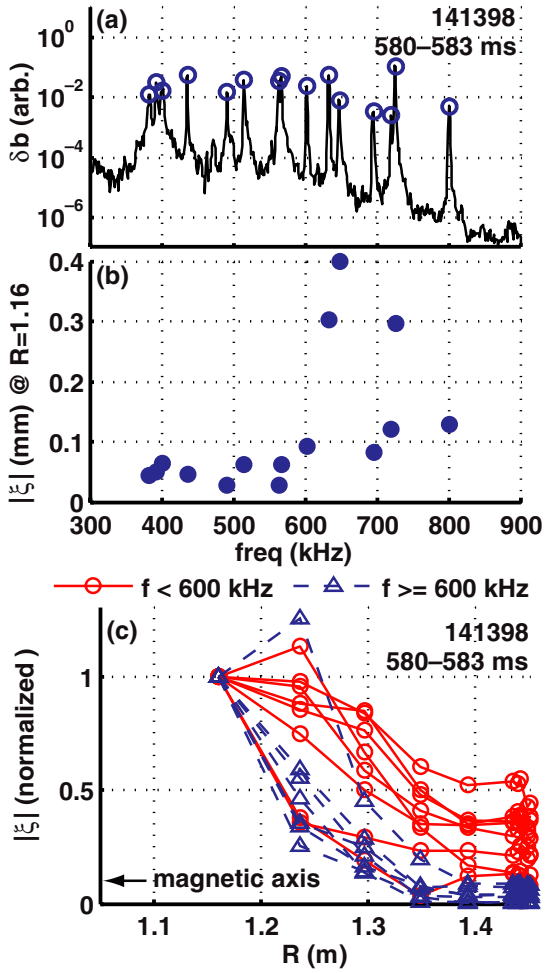

Figure 1. (*a*) δb spectrum with modes marked; (*b*) effective radial displacement ($|\xi|$) of modes at $R = 1.16$ m; and (*c*) $|\xi|$ versus R, normalized by $|\xi|$ at $R = 1.16$ m.

those discussed in [5], where high frequency AE activity was observed to correlate with enhanced core electron thermal transport. The structure measurements help distinguish CAEs from GAEs and can also be employed in modelling the effects on electron thermal transport. The observed modes are identified by comparison of their frequency and measured toroidal mode numbers with local Alfvén dispersion relations (see also [8]). The modes identified as CAEs are observed to possess higher frequencies and smaller toroidal mode numbers (i.e. smaller $|n|$) than the GAEs. Also, they are strongly core localized, in contrast with the GAEs, which also peak towards the plasma centre but have much broader radial extent.

These points are discussed in more detail in the following sections. Section 2 describes the results of the mode structure and amplitude measurements, and the diagnostics and analysis techniques used. Section 3 describes the analysis used to identify the modes as either CAEs or GAEs and the results of the analysis. Section 4 discusses the significance of the measurements and mode identification.

2. Mode-structure measurements

A spectrum of global coherent high frequency modes ($f \approx$ 400–800 kHz; $f/f_{c0} \approx 0.17$–0.33 where $f_{c0} = 2.4$ MHz is the beam ion cyclotron frequency at the magnetic axis) is observed in a high power (6 MW), beam-heated H-mode plasma (shot 141398) [8]. The modes are observed simultaneously using an array of fixed frequency reflectometers and a toroidally distributed array of poloidal magnetic field sensing coils at the plasma edge. Radial structure and amplitude measurements of the modes are obtained using the reflectometers (discussed in significant detail in [8]). The reflectometers were operated with ordinary-mode polarization at frequencies distributed over 30–75 GHz, corresponding to cutoff densities of (1.1–6.9) $\times 10^{13}$ cm^{-3}. They measured the phase shift ($\delta\phi$) of the probing millimetre-waves caused by the density fluctuations associated with the modes. For modes with large radial extent, this phase is dominated by displacement of the cutoff location caused by density fluctuations there [9], so *effective displacement*, given by $\xi = \delta\phi/2k_0$ approximates the cutoff displacement (k_0 is vacuum millimetre-wave wavenumber).

Figure 1 shows structure and amplitude for modes with frequencies in the range $f \approx$ 400–800 kHz around $t =$ 580 ms. This time is shortly after all channels of the array have begun to reflect and is coincident with a measurement of the density profile at $t = 582$ ms (see figure 5(*a*) of [8]) by the multipoint Thomson scattering (MPTS) system [10, 11]. The density profile is needed to determine cutoff locations for each channel of the array. The measurements span a significant portion of the plasma minor radius in the midplane, from major radius $R = 1.47$ m, near the plasma edge, to $R = 1.16$ m. The magnetic axis is at $R_0 = 1.05$ m. Central density continues to rise through the remainder of the shot, moving the deepest measurement location closer to the plasma edge, which makes $t = 582$ ms the optimal time for mode-structure measurements with the array. Figure 1(*a*) shows the magnetic fluctuation spectrum (δb) at the edge of the plasma. The peaks in the spectrum corresponding to the modes are marked. Figure 1(*b*) shows $|\xi|$ versus frequency at the deepest measurement location for the modes indicated in figure 1(*a*). The statistical uncertainty of the values shown in figure 1(*b*), calculated as described in [8], is smaller than the plot symbols. Figure 1(*c*) shows $|\xi|$ versus cutoff radius for each mode. For each mode, $|\xi|$ is normalized by the value of $|\xi|$ at $R = 1.16$ m so that the different mode structures may be easily compared. (It is worth noting that these structures are controlled by equilibrium density and magnetic field profiles and can be expected to evolve slowly over time as the equilibrium evolves.)

For the normalized measurements in figure 1(*c*), the statistical uncertainty (also normalized) tends to be smaller than $\pm\sim$0.05, making it comparable to or smaller than the plot symbol size. However, for the modes with small amplitude in figure 1(*b*), it can be larger near the magnetic axis, where the equilibrium density gradient is smaller, and near the edge, where the local background density fluctuation level ($\delta n/n$) is relatively large. In particular, it is larger than $\pm\sim$0.1 in about $\sim$10% of the cases and as high as $\pm\sim$0.3 in a few extreme cases.

In addition to uncertainties in the normalized amplitudes shown in figure 1(*c*), there are also uncertainties in the cutoff radii. Determining these uncertainties is a complex problem left for future work, but it is worth noting here the factors controlling the uncertainty. The cutoff radii are determined

using a radial density profile (see figure 5(a) of [8]) derived from a smoothing spline fit to the measurements of the MPTS system. Uncertainties in the fit are controlled by experimental uncertainties in the MPTS measurements. The smoothing spline algorithm [12, 13], which is routinely applied to the MPTS data (see, e.g. [11]), results in a minimum curvature cubic spline while constraining the rms deviation from the measurements to not exceed a chosen maximum value. The *smoothing parameter* (defined in [12, 13]), which controls the allowed deviation, is typically taken to be $S = N + N^{1/2}$ where N is the number of measurement points. This results in a maximum deviation comparable to the measurement uncertainty. For the plasma considered in figure 1(c), the measurements of the MPTS channels at $R \geqslant 1$ m have a relative experimental uncertainty of $\pm\sim 0.04$.

Inspection of figure 1 shows that the modes can be divided into two categories based on their frequency, amplitude and structure. Figure 1(c) shows structures for all of the modes. As can be seen, there is a group of modes that peak sharply in the core ($R <\sim 1.3$ m), and a group of modes that have significantly more radially extended structure, peaking towards the magnetic axis, but with significant amplitude at the plasma edge. The modes that peak sharply in the core have predominantly $f >\sim 600$ kHz, while those with broad structure have predominantly lower frequency. This is illustrated by the use of different line styles for the modes with $f > 600$ kHz (dashed lines) and $f < 600$ kHz (solid lines). Figures 1(a) and (b) show that modes with $f > 600$ kHz also tend to have larger $|\xi|$ at $R = 1.16$ m, and smaller δb at the plasma edge, than those with $f < 600$ kHz.

Toroidal mode numbers (n) are determined using an array of edge magnetic sensing coils that consists of ten coils irregularly toroidally distributed with separations ranging from 10° to 180°. The minimum spacing of 10° allows mode number to be determined for modes with $|n| \leqslant 18$ when a single toroidal mode number is dominant at the mode frequency, as is typically the case here. (The coils are located at toroidal angles of $\phi = 30°$, 50°, 60°, 155°, 170°, 180°, 291°, 300°, 350° and 360°.) Figure 2 shows results of the toroidal mode number identification analysis for modes in shot 141398 in the frequency range $f = 375$–850 kHz and time range $t = 400$–700 ms. For this analysis, the measured $\mathrm{d}(\delta b)/\mathrm{d}t$ for each coil is first numerically integrated and high-pass filtered with a 1 kHz cutoff. The resulting $\delta b(t)$ is divided into successive one-millisecond-long records with 50% overlap. Each record is Fourier transformed, after conditioning with a Hanning window. The result is an set of complex values, $\delta b(t, f, \phi)$, for the magnetic fluctuation at each time, frequency and coil position. Figure 2(a) shows the magnetic fluctuation level ($|\delta b|^2$ averaged over all coils) versus f and t. Figure 2(b) shows the n that best fits the array of δb values at each t and f where average $|\delta b|^2$ is large (i.e. where $\log_{10}(|\delta b|^2) >= 1$ in figure 2(a)). The best-fit n is the value which minimizes the normalized error, $\chi^2 \equiv 1 - |\sum_{\forall\phi} \delta b \mathrm{e}^{-\mathrm{i}n\phi}|^2/(N_\phi \sum_{\forall\phi} |\delta b|^2)$, where $N_\phi = 10$ is the number of coils. Figure 2(c) shows χ^2 for the fits in figure 2(b). The normalized error can be interpreted as the fraction of observed fluctuation power (i.e. $\sum_{\forall\phi} |\delta b|^2$) that cannot be explained by a single toroidal harmonic. As can be seen in figure 2(c), typically $\chi^2 <\sim 0.5$, indicating that a single toroidal harmonic is dominant.

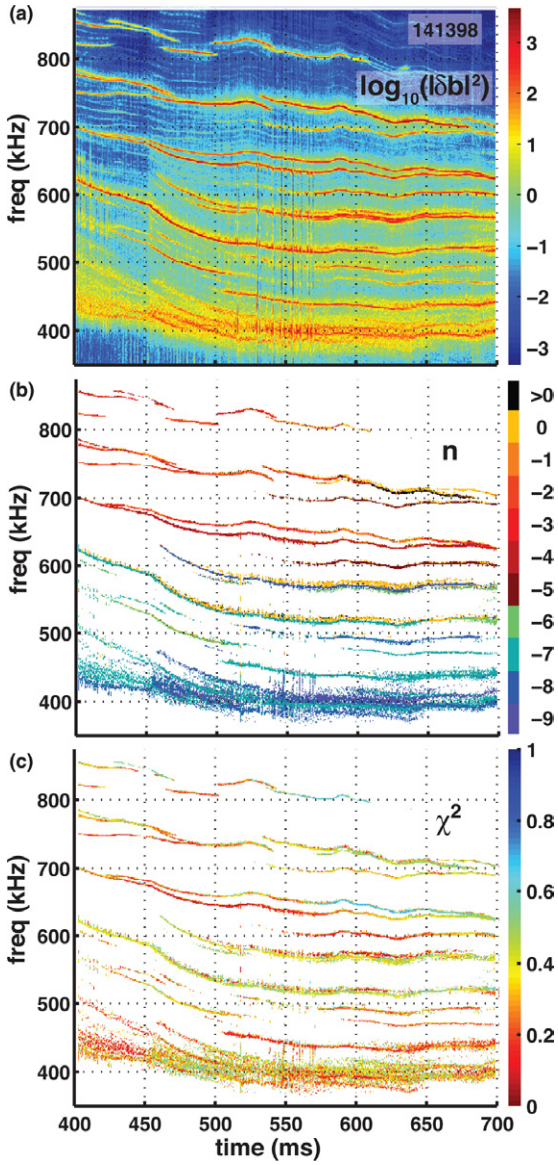

Figure 2. (a) δb spectrum with CAEs and GAEs; (b) best-fit toroidal mode number n at each t and f with large δb; and (c) normalized error χ^2 of n fit.

From inspection of figure 2(b), it can be seen that the two groups of modes identified from figure 1 have distinctly different ranges of n (with some minor exceptions discussed below). The modes with $f >\sim 600$ kHz at $t \sim 580$ ms tend to have $|n| \leqslant 5$. In contrast, those with $f <\sim 600$ kHz predominantly have $n = -6$ to -8. Both groups of modes predominantly have $n \leqslant 0$, where $n < 0$ indicates propagation counter to the neutral beams. (The sign convention used is such that for a given n, $\delta b(t, \phi) \propto \cos(\omega t + n\phi)$. Toroidal angle ϕ increases in the direction of the toroidal magnetic field. The neutral beams inject in the same direction, toroidally, as the flow of the plasma current and the rotation of the plasma, which is opposite the direction of the toroidal magnetic field.)

There are, as indicated, minor exceptions to the pattern of mode numbers identified for each group of modes. For instance, weak $n = 0$ sidebands appear $\sim$5 kHz above two long-lived modes with frequencies between $f = 500$ and

600 kHz. The cause of these sidebands is not clear. Possibly they are nolinearly driven, as might be conjectured from the way their frequencies evolve relative to nearby larger amplitude modes. Another exception is an $f \sim 815$ kHz mode at $t = 650$ ms with a best-fit $n > 0$. Inspection of figure 2(*a*) shows several peaks around $f \sim 815$ kHz with frequencies apparently evolving to cross through each other between $t = 550$ and 700 ms. This would interfere with mode number identification because there would be no dominant n. Figure 2(*c*) shows a relatively large χ^2 for this mode number identification. While these and the other exceptions bear further investigation in the future, the overall pattern of mode numbers identified for each group of modes remains clear.

3. Identification of modes

The modes shown in figure 1 are identified using f and measured n. Modes in NSTX with n and f in the observed range, where f is a significant fraction of the beam ion cyclotron frequency, and the observed propagation is counter to the neutral beams, have historically been identified as a mixture of CAEs and GAEs excited by Doppler-shifted cyclotron resonance with beam ions [1–3, 7]. However, distinguishing GAEs from CAEs has sometimes proven difficult [3]. In order to facilitate making this distinction, an analysis is presented that utilizes f and measured n in conjunction with local Alfvén dispersion relations (see also [8]). Using this analysis, the group of strongly core-peaking modes with predominantly $f >\sim 600$ kHz are clearly identified as CAEs, while the group of broad structure modes with predominantly $f <\sim 600$ kHz are identified as GAEs.

The local dispersion relationship for compressional Alfvén waves, $\omega^2 \sim k^2 V_A^2$, can be used to establish minimum requirements on ω and n for a CAE to exist. For $n \neq 0$, CAEs should be localized within a 'well' in the R–Z plane where $(n^2/R^2)V_A^2 - \omega^2 < 0$, inside of which compressional Alfvén waves can propagate but outside of which they are evanescent. This requirement applies in the plasma frame, so in the presence of a Doppler shift due to toroidal rotation the requirement becomes $(n^2/R^2)V_A^2 - (\omega - 2\pi n f_{ROT})^2 < 0$. Figure 3(*a*) shows $(n^2/R^2)V_A^2 - (\omega - 2\pi n f_{ROT})^2$ for the mode with $f = 633$ kHz and $n = -4$ at $t = 582$ ms in shot 141398. Of course, for an eigenmode to fit inside the well, the R–Z 'wavelength' inside the well, $\lambda_{R-Z} = 2\pi[(\omega - 2\pi n f_{ROT})^2]/V_A^2 - n^2/R_0^2]^{-1/2}$, should be comparable to or smaller than the well width. (In fact, the exact limit for the largest value of λ_{R-Z} depends on the shape of the well. For instance, for a square well, the maximum would be twice the well width. For parabolic wells there is a different factor.) The modes are compared with this requirement using measurements of equilibrium electron density from MPTS and magnetic field from LRDFIT[5] equilibrium reconstruction [14, 15] using motional Stark effect [16] measurements of magnetic field pitch. The Doppler shift due to toroidal rotation is determined using charge exchange recombination spectroscopy [17]. Figure 3(*b*) shows the radial width of the well in the midplane versus frequency for $n = -3$ to -8, for frequencies in the range $f = 400$–800 kHz. It also shows

[5] http://w3.pppl.gov/~jmenard/software/lrdfit/lrdfit-index.htm.

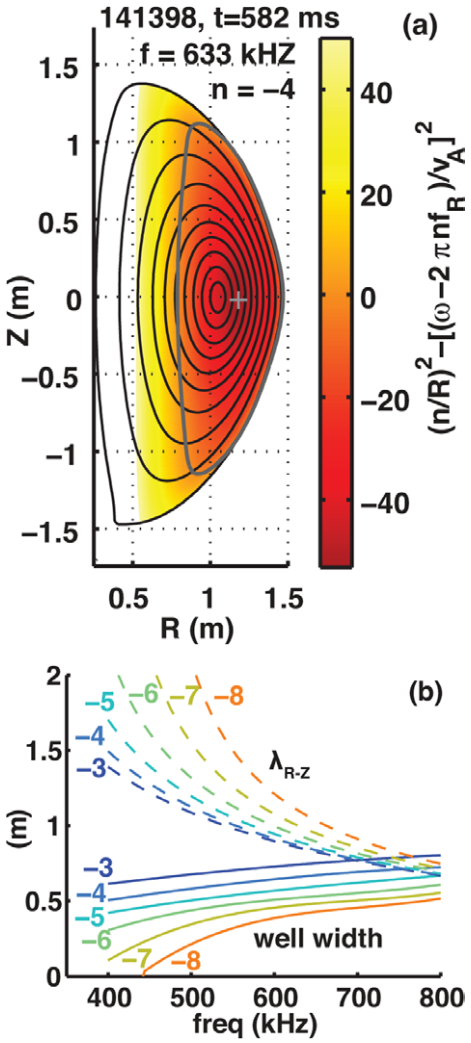

Figure 3. (*a*) Shading shows $(n^2/R^2)V_A^2 - (\omega - 2\pi n f_{ROT})^2$ for $n = -4$ $f = 633$ kHz, in shot 141398 at $t = 582$ ms. Region of negative value, bounded by thick grey contour, forms CAE 'well'. Deepest point of well marked by '+'. Black contours show plasma flux surfaces; (*b*) wavelength, λ_{R-Z}, at deepest point of well (dashed lines) and radial width of well in midplane (solid lines) for different n.

λ_{R-Z} versus frequency for the same n, calculated at each frequency and n at the deepest point of the well (i.e. using the most negative value of $(n^2/R^2)V_A^2 - (\omega - 2\pi n f_{ROT})^2$ in the R–Z plane). The figure shows that λ_{R-Z} is very large at low frequency, decreasing rapidly with increasing frequency and approaching the value of the well width only at the highest frequencies, indicating that an eigenmode is likely able to fit within the well only at the higher frequencies. Well width is smaller at lower frequencies, further enhancing the disparity between λ_{R-Z} and well width, reinforcing this expectation. Notably, well width decreases with increasing n, while λ_{R-Z} increases with increasing n, indicating that an eigenmode is likely able to fit within the well only at low enough n. These sensitivities to frequency and n indicate that the $f >\sim 600$ kHz modes have high enough frequencies and low enough $|n|$ that an eigenmode is likely able to fit within the well. In contrast, for some of the $f <\sim 600$ kHz modes, $(n^2/R^2)V_A^2 - (\omega - 2\pi n f_{ROT})^2 > 0$ everywhere,

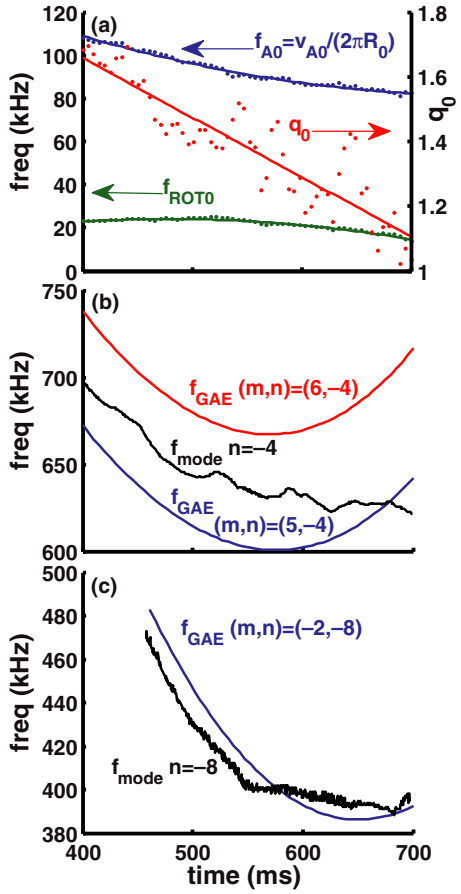

Figure 4. (*a*) Measurements (dots) of Alfvén frequency, f_{A0}, toroidal rotation, f_{ROT0} and safety factor, q_0, at R_0 and polynomial fits (solid lines) to measurements; GAE frequency, f_{GAE}, compared with frequency of (*b*) '$f = 633$ kHz' and (*c*) '$f = 401$ kHz' modes (see figure 1).

while for the others, λ_{R-Z} is significantly larger than the well width.

Comparison of long-term frequency evolution (figure 2(*a*)) with expectation for GAEs (also discussed in some detail in [8]) also proves informative. GAEs peak near a minimum of the Alfvén continuum (e.g. at R_0) and have $\omega \approx |k_{||}|V_A$ (in the plasma frame), where $k_{||} \approx (m/q - n)/R$. The modes in figure 1 peak near R_0, so the GAE frequency (f_{GAE}) is calculated using the values of safety factor (q_0), Alfvén frequency ($f_{A0} = V_{A0}/2\pi R_0$) and toroidal rotation (f_{ROT0}) at R_0, which are shown in figure 4(*a*). The points in the figure show the measured values and the solid lines show least-squares polynomial fits. Figure 4(*b*) illustrates the analysis for the $n = -4$ mode with $f = 633$ kHz at $t = 582$ ms. The polynomial fits shown in figure 4(*a*) are used to calculate f_{GAE}. The analysis shows that the mode frequency appears to evolve inconsistently with f_{GAE} assuming either of the poloidal mode numbers, $m = 5$ or 6, that give the best-fit to the mode frequency. This is largely due to a high sensitivity to q_0 variation. The small $|n|$ mandates a large poloidal mode number, m, to fit the observed frequency. The frequencies of the other $f >\sim 600$ kHz modes also evolve inconsistently with f_{GAE}. In contrast, the lower frequency modes have frequency evolution consistent with f_{GAE}. They tend to have large $|n|$, leading to small m, so f_{GAE} is relatively insensitive to q_0 variation. Figure 4(*c*) illustrates the analysis for the $n = -8$ mode with $f = 401$ kHz at $t = 582$ ms. The analysis shows that the mode frequency evolves consistently with f_{GAE} assuming $m = -2$.

4. Discussion

The mode-structure measurements presented here were obtained in a plasma very similar to those discussed by Stutman *et al* [5], in which high frequency AE activity is shown to correlate with enhanced core electron thermal transport. Stutman *et al* [5] posited that the high frequency AEs caused the transport by stochasticization of resonant electron orbits in the presence of multiple modes (see also [18]). They noted that the modes may 'resonantly couple to the bulk (∼1 keV energy), primarily trapped electron population', because they have frequencies comparable to the characteristic trapped electron bounce frequency of 0.6 MHz.

The structure measurements presented here show that the high frequency AEs tend to peak in the plasma core. This is consistent with a key element supporting the hypothesis of Stutman *et al* [5], which was their expectation that the modes peaked in the plasma core where the enhanced transport occurred. Although structure measurements were not available, they identified the modes as GAEs—which are theoretically expected to peak in the plasma core—based on their frequencies and on signatures in the time-dependent mode spectrum.

In contrast with Stutman *et al* [5], however, analysis presented here indicates that some of the modes are, in fact, CAEs instead of GAEs. The distinction is significant for several reasons. First, the two types of modes have very different effects on resonant particle orbits. For instance, in contrast with GAEs, CAEs localized in the core of the plasma will have a significant parallel magnetic field fluctuation in the core that will perturb the pitch angle of resonant electrons. Fully understanding the implications of this and other differences in orbital effects will require future investigation.

A second motivation for distinguishing CAEs from GAEs stems from the potential use of mode-structure measurements to predict the resulting electron thermal transport. Gorelenkov, *et al* showed [18] how the magnetic perturbation structures of a spectrum of high frequency AEs could be used as input to the guiding centre orbit code ORBIT to make such a prediction. In order to test the hypothesis of Stutman *et al* [5], they calculated the transport that would result from a spectrum of GAEs. In performing the calculation, they used *ad hoc* GAE structures motivated by phenomenological considerations as inputs for ORBIT. In principle, however, the mode-structure measurements presented here could be used to derive a more physically accurate set of magnetic perturbation structures, specific to the plasma under investigation, as inputs for ORBIT. It is here that the distinction between GAEs and CAEs becomes significant. The structure measurements are sensitive to density perturbations. The plasma flows that cause the density perturbations are primarily due to $E \times B$ motion, so the measurements can be used to determine the electric, and associated magnetic, perturbation of the modes. (Displacement parallel to the equilibrium magnetic

field, which is largely due to the acoustic response of the plasma, is expected to be negligible at the high frequencies of the observed modes.) However, the relationship between the density and flow perturbations is different for CAEs and GAEs. For AEs with primarily shear Alfvén polarization, such as GAEs, the density perturbation results from radial displacement of the equilibrium density gradient in the region where the mode is localized. On the other hand, for AEs with primarily compressional Alfvén polarization, such as CAEs, compression also contributes significantly to the density perturbation in the region where the mode is localized. Consequently, interpretation of the measured structures to obtain inputs for ORBIT benefits from the determination of mode polarization that results from distinguishing CAEs from GAEs. Extending the analysis of Gorelenkov *et al* [18] to incorporate the mode structures presented here is left as an exercise for future investigation.

A significant result of the transport modelling of Gorelenkov *et al* [18] was a prediction of the total GAE fluctuation level necessary to cause the level of electron thermal transport observed by Stutman *et al* [5]. Although the transport modelling assumed a spectrum of GAEs with *ad hoc* structures differing significantly from the measured structures, it is informative to compare the measured mode amplitudes with this prediction. The predicted fluctuation level is expressed in terms of the parameter $\alpha = \delta A_{||}/B_0 R_0$, where $\delta A_{||}$ is the parallel component of the perturbed vector potential. The fluctuation level required to explain the observed electron thermal transport is $\alpha = 4 \times 10^{-4}$. For the modes identified here as GAEs, the total value of α at $R = 1.16$ m can be estimated by summing over values estimated for each of the individual modes. For GAEs, α is related to the radial plasma displacement, ξ_r, by the expression $\xi_r = \delta B_r/\mathrm{i}k_{\|}B_0 = \alpha R_0 k_\theta / k_{\|}$ [18]. The measured effective displacement at $R = 1.16$ m (figure 1(*b*)) is used as an estimate of ξ_r. Values for $k_{||}$ are estimated from the GAE dispersion relation, $\omega \approx |k_{||}|V_A$, using measured V_A at R_0 (figure 4(*a*)) and correcting for a toroidal Doppler shift using the measured n and f_{ROT0} (figure 4(*a*)). Values for $k_\theta = m/r$ are determined by estimating effective values of m at R_0 via the relation $k_{||} \approx (m/q - n)/R$, using the measured values of n and q_0 (figure 4(*a*)). The resulting values have magnitudes in the range $|m| \approx 1/2$–$2\ 1/2$. The value for r is taken to be $r = (1.16\,\mathrm{m} - R_0) = 0.11$ m. The result of this analysis gives a total GAE fluctuation level of $\alpha = 3.4 \times 10^{-4}$ at $R = 1.16$ m, which is comparable to the predicted value required to explain the observed electron thermal transport. There are, of course, significant approximations used in this analysis, so a more careful analysis is warranted as a part of future investigation. Also, an approach must be developed for predicting the contribution of the CAEs to the transport.

Another significant result of the transport modelling of Gorelenkov *et al* [18] was a prediction that the level of transport caused by the spectrum of modes was extremely sensitive to the number of modes. The modelling showed a sharp increase in the level of transport when the number of modes reached a threshold of ∼15, which is equal to the total number of modes observed in the range $f \sim 400$–800 kHz. Of course, some of those modes are identified to be CAEs, while the modelling considered only GAEs. Further work is necessary to evaluate the mode number threshold for a spectrum including both CAEs and GAEs.

Another important area for future investigation will be to compare the mode-structure measurements presented here with predictions from theory. Belova *et al* [19] are currently engaged in theoretical modelling of the CAE/GAE spectrum expected for the plasma investigated here using the hybrid kinetic and MHD code, HYM. Modes from the simulations that have been validated by measurements can then be incorporated into the type of analysis used by Gorelenkov *et al* [18] to further refine the prediction of electron thermal transport.

In conclusion, a spectrum of high frequency AEs is observed in a high power, beam-heated H-mode NSTX plasma [8] similar to those in which high frequency AE activity is shown by Stutman *et al* [5] to correlate with enhanced core electron thermal transport. An analysis is presented using local dispersion relations in combination with mode frequency and measured toroidal mode number to show that some of the modes are GAEs and, in contrast with the identification of Stutman *et al*, some of the modes are CAEs. Stutman *et al* posited that the high frequency AEs caused the transport by stochasticization of resonant electron orbits in the presence of multiple modes. The observed spectrum is shown to be consistent with an analysis by Gorelenkov *et al* [18] that predicts the number of modes and total fluctuation level required to cause the thermal transport observed in the plasmas investigated by Stutman *et al* However, the analysis of Gorelenkov *et al*, which was based on electron orbit modelling, assumed a spectrum of GAEs with phenomenologically motivated *ad hoc* structures as inputs. GAEs and CAEs can have very different effects on resonant electron orbits, so further investigation is warranted extending the analysis to incorporate a mixed spectrum of CAEs and GAEs. Also, the measured structures reported here can, in principle, be used to provide a more physically accurate set of magnetic perturbation inputs to the orbit modelling.

Acknowledgments

The authors are grateful to the NSTX team for supporting these experiments. This work was supported by US DOE Contracts DE-FG02-99ER54527 and DE-AC02-09CH11466.

References

[1] Heidbrink W.W., Fredrickson E.D., Gorelenkov N.N., Rhodes T.L. and Van Zeeland M.A. 2006 *Nucl. Fusion* **46** 324–34
[2] Fredrickson E.D., Gorelenkov N.N. and Menard J. 2004 *Phys. Plasmas* **11** 3653–9
[3] Fredrickson E.D. *et al* 2011 *Proc. 38th EPS Conf. on Plasma Physics (Strasbourg, France, 27 June–1 July 2011)* vol 35G (ECA) P2.119 http://ocs.ciemat.es/EPS2011PAP/pdf/P2.119.pdf
[4] Fredrickson E.D. *et al* 2012 *Nucl. Fusion* **52** 043001
[5] Stutman D., Delgado-Aparicio L., Gorelenkov N., Finkenthal M., Fredrickson E., Kaye S., Mazzucato E. and Tritz K. 2009 *Phys. Rev. Lett.* **102** 115002
[6] Gates D.A., Gorelenkov N.N. and White R.B. 2001 *Phys. Rev. Lett.* **87** 205003
[7] Gorelenkov N.N., Fredrickson E., Belova E., Cheng C.Z., Gates D., Kaye S. and White R. 2003 *Nucl. Fusion* **43** 228–33

[8] Crocker N.A. *et al* 2011 *Plasma Phys. Control. Fusion* **15** 105001
[9] Nazikian R., Kramer G.J. and Valeo E. 2001 *Phys. Plasmas* **8** 1840–55
[10] Leblanc B.P., Bell R.E., Johnson D.W., Hoffman D.E., Long D.C. and Palladino R.W. 2003 *Rev. Sci. Instrum.* **74** 1659–62
[11] Leblanc B.P., Diallo A., Labik G. and Stevens D.R. 2012 *Rev. Sci. Instrum.* **83** 10D527
[12] Reinsch C.H. 1967 *Numer. Math.* **10** 177–83
[13] Reinsch C.H. 1971 *Numer. Math.* **16** 451–4
[14] Menard J.E. *et al* 2006 *Phys. Rev. Lett.* **97** 095002
[15] Levinton F.M. *et al* 2007 *Phys. Plasmas* **14** 056119
[16] Levinton F.M. and Yuh H. 2008 *Rev. Sci. Instrum.* **79** 10F522
[17] Bell R.E. and Feder R. 2010 *Rev. Sci. Instrum.* **81** 10D724
[18] Gorelenkov N.N., Stutman D., Tritz K., Boozer A., Delgado-Aparicio L., Fredrickson E., Kaye S. and White R. 2010 *Nucl. Fusion* **50** 084012
[19] Belova E.V., Gorelenkov N.N., Fredrickson E.D., Berk H.L., Kramer G.J. and Medley S.S. 2012 Numerical simulations of NBI-driven GAE modes in L-mode and H-mode discharges in NSTX *Proc. 24th Int. Conf. on Fusion Energy 2012 (San Diego, CA, 8–13 October 2012)* (Vienna: IAEA) paper TH/P6–16 submitted http://fec2012.iaea.org/contributionDisplay.py?contribId=302&sessionId=9&confId=10